RSC Advances

ROYAL SOCIETY OF CHEMISTRY

www.rsc.org/advances

Facile preparation of $Ag/AgVO_3/BiOCl$ composite and its enhanced photocatalytic behavior for methylene blue degradation

Lei Zhang [a, b], Xingzhong Yuan [a, b *], Hou Wang [a, b], Xiaohong Chen [c], Zhibin Wu [a, b], Yang Liu [a, b], Shansi Gu [a, b], Qian Jiang [a, b], Guangming Zeng [a, b]

[a] *College of Environmental Science and Engineering, Hunan University, Changsha 410082, PR China*

[b] *Key Laboratory of Environment Biology and Pollution Control, Hunan University, Ministry of Education, Changsha 410082, PR China*

[c] *Collaborative Innovation Center of Resource-Conserving & Environment-friendly Society and Ecological Civilization, Changsha 410083, PR China*

[*] Corresponding author at: College of Environmental Science and Engineering, Hunan University, Changsha 410082, PR China. Tel.: +86 731 88821413; fax: +86 731 88823701.
E-mail address: yxz@hnu.edu.cn (X.Z. Yuan)

Abstract

BiOCl and $AgVO_3$ have aroused great interests as photocatalysts in environmental remediation. They could be modified with each other to improve the photocatalytic activity. A novel $Ag/AgVO_3/BiOCl$ composite photocatalyst was initiated via a facile ultrasound assisted hydrothermal method. The as-prepared samples were characterized by X-ray diffraction (XRD), X-ray photoelectron spectroscopy (XPS), Scanning electron microscopy (SEM), Transmission electron microscopy (TEM), UV-vis diffuse reflectance spectroscopy (UV-DRS), Photoluminescence (PL) emission spectroscopy and Brunauer Emmett Teller (BET) specific surface area analysis. It is revealed that the $Ag/AgVO_3/BiOCl$ composite was successfully synthesized with large specific surface area, mesoporous structure, enhanced light absorption performance and good recyclability. The photocatalytic activity for methylene blue (MB) degradation was investigated under visible light irradiation. The $Ag/AgVO_3/BiOCl$ composite photocatalyst exhibited superior photocatalytic activity, and about 93.16% of MB was removed within 60 minutes irradiation, which was better than that of pure BiOCl (29.24%) and $Ag/AgVO_3$ (37.52%). The enhanced photocatalytic activity could be attributed to the effective visible light absorption and separation of electrons and holes. Therefore, it is reasonable to believe that the $Ag/AgVO_3/BiOCl$ composite photocatalyst has great potentiality in environmental remediation.

Keywords: $Ag/AgVO_3/BiOCl$ composite; Photocatalytic activity; Visible light; Methylene blue

1. Introduction

With the development of urbanization and industrialization, environmental problems have become increasingly serious.[1] Photocatalysis based on semiconductors has been investigated due to the demand for organic dyes degradation.[2-4] Organic dyes, like methylene blue (MB) and methyl orange (MO), are toxic and hardly decompose quickly.[5-7] Photocatalytic degradation of MB is of high performance and cost-effective, it seldom discharges any perilous chemicals.[8] It provided a promising way to meet the challenges in environment, energy and sustainability.[9] Many semiconductors like TiO_2, ZnO have been extensively utilized as effective photocatalysts for organic dyes degradation.[10, 11] However, TiO_2 has a few major drawbacks on its photoexcitation domain.[12] Recently, bismuth oxychloride (BiOCl) has been studied due to its outstanding photocatalytic performance and environmental properties.[13] It has been reported that BiOCl exhibited better performance than TiO_2 for the Rhodamine B (RhB) degradation.[14] BiOCl is a p-type semiconductor with a wide bandgap about 3.12 eV.[15-17] The highly anisotropic layered structure featured as $[Bi_2O_2]^{2+}$ layers being sandwiched between two slabs of chloride ions could also efficiently induce the separation of photo-generated electron-hole pairs and enhance the photocatalytic activity.[18, 19] So far, it has been reported that doped-BiOCl with other materials could surprisingly enhance the photocatalytic performance than that of pure BiOCl. *Duo et al.* reported a photocatalytic activity for the MO degradation by $BiPO_4$/BiOCl heterojunction composites.[16] *Cao et al*. reported BiOCl/m-$BiVO_4$ composites for RhB degradation.[20] *Zuo et al.* studied BiOCl/Bi_2MoO_6 composites

with the photocatalytic activity in degrading MO.[21] In our previous study, *Liu et al*. synthesized a three-dimensional $BiOCl_{0.75}Br_{0.25}$/graphene microsphere for RhB degradation.[22] However, due to its wide bandgap, BiOCl is not available for visible light irradiation, which limited its practical applications.[5, 23] It is essential to modify BiOCl by coupling with another narrow-bandgap material to improve the visible light absorption and promote the separation of photogenerated electron-hole pairs.[3]

Silver vanadium oxides (SVOs) such as $AgVO_3$ (α-$AgVO_3$ and β-$AgVO_3$), $Ag_2V_4O_{11}$, Ag_3VO_4 and $Ag_4V_2O_7$ have attracted more and more attention owing to their perfect electrical conductivity and potential applications in photocatalysts. For SVOs, the unique hybridization of valence bands lead to a narrow bandgap, this makes it a potential application as visible-light-sensitive photocatalyst.[24, 25] Typically, β-$AgVO_3$ exhibited much higher charge capacity than α-$AgVO_3$.[26] However, its low capability of separating electron-hole pairs became one of limitations for its practical application.[26, 27] Modified Ag nanoparticles could improve the separation of electrons and holes and enhance the absorption of the materials in the visible light, resulting in better photocatalytic performance.[28, 29] The report about the synthesis and application of Ag/$AgVO_3$/BiOCl composite is still scarce.

In this study, we demonstrated a facile approach to prepare a novel Ag/$AgVO_3$/BiOCl composite photocatalyst via a facile ultrasound assisted hydrothermal method. The photocatalytic activity of Ag/$AgVO_3$/BiOCl composite was measured by the degradation of MB under visible light irradiation. A feasible mechanism for the MB degradation was proposed. Cycling experiments for five turns

were carried out to verify the stability of $Ag/AgVO_3/BiOCl$ composite.

2. Experimental

2.1 Materials

Bismuth nitrate pentahydrate ($Bi(NO_3)_3 \cdot 5H_2O$) was purchased from Xi long Chemical Co., Ltd. Silver nitrate ($AgNO_3$) was purchased from Sinopharm Chemical Reagent Co., Ltd. Ammonium metavanadate (NH_4VO_3) was purchased from Shanghai Shan Pu Chemical Co., Ltd. Sodium hydroxide (NaOH) and Ethanol absolute were purchased from Tianjin Hengxing Chemical Reagent Co., Ltd. Hydrochloric acid (HCl) was purchased from Zhuzhou City Star Glass Co., Ltd. All reagents were of analytical grade and used directly without further purification.

2.2 Synthesis of $AgVO_3/BiOCl$ composite

The BiOCl was prepared by a modified method.[30] Typically, 1.940 g $Bi(NO_3)_3 \cdot 5H_2O$ was dissolved in 20 ml HCl of 1.5 mol/L to get a transparent solution. Then, 0.72 mol/L of NaOH was added dropwise into the above solution with constant stirring until precipitations were appeared in the mixed solution. Then the mixed solution was stirred for 10 minutes. Finally, the precipitates were filtrated and washed for several times with deionized water, followed by drying at 80°C overnight.

Then, different stoichiometric amounts of as-prepared BiOCl were dispersed in 20 mL of deionized water with the aid of ultrasonication. $Ag/AgVO_3/BiOCl$ composite was synthesized via a hydrothermal method[27]: 20 mL of 0.11 mol/L $AgNO_3$ solution and 20 mL of 0.10 mol/L NH_4VO_3 solution were successively added to the BiOCl suspension and the mixture was stirred for 180 min. The obtained mixture was

transferred into a Teflon-lined stainless steel autoclave with heated at 180°C for 24 h. The system was then allowed to cool down to room temperature naturally. The collected product was centrifuged and washed with deionized water and absolute ethanol four times, and then dried under vacuum at 80°C. For comparison, the un-doped $Ag/AgVO_3$ was also prepared by the same procedure without the addition of BiOCl. The as-synthesized $Ag/AgVO_3$/BiOCl composite was labeled as AB2.5, AB5.0 and AB10.0 with 2.5, 5.0 and10.0 wt% of BiOCl to $Ag/AgVO_3$, respectively.

2.3 Characterization

X-ray powder diffraction (XRD) patterns of the samples were obtained by a Rigaku D/Max 2500 diffractometer with Cu Kα radiation (λ=1.5406 Å) under 40 kV, 250 mA. The surface elemental composition analyses were conducted by the X-ray photoelectron spectroscopy (XPS) spectra on a Thermo ESCALAB 250Xi instrument. The surface morphologies of the samples were observed by scanning electron microscopy (SEM) with a model of HITACHI S4800 machine. The transmission electron microscopy (TEM) images were obtained by FEI TECNAI G2-F20 machine. UV-Visible diffused reflectance spectra (UV-DRS) of the samples were carried out on a Hitachi UV-3310 diffuse reflection instrument. The photoluminescence (PL) spectra of the photocatalysts were obtained by a F4600 (Hitachi, Japan) photoluminescence detector with an excitation wavelength of 384 nm. The Brunauer Emmett Teller (BET) specific surface area and total pore volume of the samples were measured by nitrogen adsorption-desorption analysis with an automatic Micromeritics 3 Flex instrument.

2.4 Photocatalytic experiment

The photocatalytic degradation of MB was carried out in a 250 mL beaker containing 100 mL MB solution (7 mg/L) and photocatalyst (50 mg). The source of visible light irradiation was generated by a 300 W Xenon lamp (14V, 16A) with a 420 nm cutoff filter. The mixed solution was magnetically stirred in the dark for 1 h to reach adsorption-desorption equilibrium. Then the solution was exposed to visible light with continuous stirring. At certain time intervals, a certain amount of liquid were collected and centrifuged at 8000 rpm for 10 min to remove the photocatalyst particles. The concentration of residual liquid was analyzed by a UV-vis spectrophotometer (UV-2550, SHIMADZU Corporation, Japan) at its maximum absorption wavelength of 664 nm.

3. Results and discussion

3.1 XRD analysis

The purity and crystallinity of as-prepared samples were confirmed by X-ray diffraction (XRD) and depicted in Fig. 1. For $Ag/AgVO_3$, all peaks are attributed to the monoclinic phase of β-$AgVO_3$ (JCPDS No. 29-1154) and the face-centered cubic Ag (1 1 1) phase (JCPDS No. 04-0783).[27] For BiOCl, all peaks could be well indexed as tetragonal phase of BiOCl (JCPDS No. 06-0249).[31] And the intensity of BiOCl characteristic peaks is weak due to the low proportion of BiOCl to $Ag/AgVO_3$.[20] The result indicates that $Ag/AgVO_3$/BiOCl composite is well crystallized and prepared successfully.

3.2 XPS analysis

X-ray photoelectron spectroscopy (XPS) measurements were carried out to determine the surface chemical composition and oxidation states of elements for as-prepared samples. The XPS survey spectrum of AB5.0 sample was shown in Fig. 2a. Chemical binding energies observed at approximately 530.18 eV, 159.43 eV, 198.51 eV, 368.01 eV and 517.03 eV are assigned to O 1s, Bi 4f, Cl 2p, Ag 3d and V 2p, respectively, which suggests that the AB5.0 composite are composed of O, Bi, Cl, Ag and V elements.[27] C 1s peak can be ascribed to the adventitious hydrocarbon from XPS instrument itself.[17, 32] In Fig. 2b, the O 1s region is matched with two peaks at 530.2 eV and 532.0 eV. The main peak at 532.0 eV is related to the binding energy of Bi-O bonds in $[Bi_2O_2]^{2+}$ layered structure of BiOCl.[22, 33] The peak at 530.2 eV is assigned to the binding energy of V-O in the $AgVO_3$ system.[34, 35] In Fig. 2c, the peaks at 164.73 eV and 159.44 eV are assigned to the binding energies of Bi $4f_{5/2}$ and Bi $4f_{7/2}$ spin-orbital splitting photoelectrons of Bi^{3+} in the BiOCl chemical state.[16, 36] In Fig. 2d and Fig. S1, the peaks at 198.14 eV and 199.75 eV are assigned to the binding energies of Cl $2p_{3/2}$ and Cl $2p_{1/2}$ spin-orbital splitting photoelectrons of Cl^- in the BiOCl chemical state.[36, 37] However, the shift of 0.36 eV to the higher binding energies of 198.50 eV and 200.14 eV are observed in AB5.0 composite, implying that the chemical surroundings of Cl^- have changed.[33] This tiny shift indicates that Ag^+ (or $AgVO_3$) has doped into the lattices of BiOCl.[16, 34, 36] From the XPS spectra of Ag 3d in Fig. 2e, two peaks at 368.1 eV and 374.1 eV are assigned to the binding energies of Ag^+ $3d_{5/2}$ and Ag^+ $3d_{3/2}$, two peaks at 368.5 eV and 374.6 eV are assigned to the

binding energies of Ag^0 $3d_{5/2}$ and Ag^0 $3d_{3/2}$.[28, 34] In Fig. 2f, two peaks at 517.08 eV and 524.41 eV are assigned to the binding energies of V^{5+} $2p_{5/2}$ and V^{5+} $2p_{3/2}$ in the $Ag/AgVO_3$.[26, 28] The result indicates the successful preparation of AB5.0 composite.[26]

3.3 SEM and TEM analysis

The morphology of as-prepared samples was determined by SEM and TEM analysis. As shown in Fig. 3a, the typical SEM image of pristine BiOCl exhibits agminated flower-like microspheres with the diameter of 400-500 nm, and the microsphere is composed of many thin nanosheets. This morphology is different from conventional BiOCl bulk plates architectures[16]. In Fig. 3b, the SEM image displays an overall view of $Ag/AgVO_3$ microrods with the length of 4-10 μm and the width of 270-300 nm. Fig. 3c shows the morphology of AB5.0 composites. Some irregular shaped particles are successfully deposited on the surface of $Ag/AgVO_3$ microrods. Then samples were further characterized by TEM analysis. As shown in Fig. 3d-e, the typical TEM image further reveals that the flower-like structure is constructed by nanosheets with an average thickness of 6-10 nm.[36, 38] In addition, the chemical composition of the samples is confirmed by X-ray energy dispersive spectroscopy (EDS) analysis. Fig. 3f proves the presence of O, Bi, Cl, Ag and V elements. The atomic ratio (At %) of every element is shown in Table. S1. The result is in agreement with XRD results.

3.4 UV-vis diffuse reflectance spectroscopy analysis

The optical absorption property is one of the most important properties to characterize the optical property of semiconductor. UV-visible diffuse reflectance

spectra in the wavelength range of 200-700 nm for the $Ag/AgVO_3$, BiOCl and $Ag/AgVO_3$/BiOCl composite are shown in Fig. 4a. The absorption edge of BiOCl is located at around 400 nm, while $Ag/AgVO_3$ has a broad absorption scale over the whole visible light region. For $Ag/AgVO_3$/BiOCl composite, the absorption edge exhibits red-shift to visible light region until 600 nm, and the intensity increases than that of BiOCl. Moreover, the absorbance is higher than that of $Ag/AgVO_3$ in the high wavelength region (600-800 nm), and the slopes of these two curves are different. This could be attributed to integrative effect of the $Ag/AgVO_3$ microrods formed on the surfaces of the BiOCl microspheres.[27] Compared with other samples, the $Ag/AgVO_3$/BiOCl composite has remarkable enhancement of the absorption intensity and the extension of the edge in the visible light region, implying that $Ag/AgVO_3$/BiOCl composite can be used as an excellent photocatalyst under visible light irradiation.[9, 10] The bandgap energy could be calculated by the following formula[35]:

$$\alpha h\nu = A(h\nu - Eg)^{n/2} \qquad (1)$$

Where *α, v, Eg* and *A* are the absorption coefficient, light frequency, the bandgap energy, and a constant, respectively. *n* is determined by the type of optical transition of a semiconductor (*n*=1 for a direct transition and *n*=4 for an indirect transition). For BiOCl and $AgVO_3$, the value of *n* is 4 and 1, respectively. As illustrated in Fig. 4b-c, the bandgap energy of as-prepared BiOCl and $Ag/AgVO_3$ is estimated to be 3.12 eV and 2.10 eV, respectively, from the intercept of the tangent to the line. The result is in agreement with former reports.[16, 27]

3.5 Nitrogen adsorption-desorption analysis

The specific surface area and total pore volume of the samples were measured by nitrogen adsorption-desorption analysis, and the corresponding curves are shown in Fig 5. Inset showed the corresponding pore-size distribution, which implied the presence of mesoporous in the size range of 2-50 nm.[22] The mesoporous structure is more efficient for the photocatalytic degradation of organic pollutants in water.[35, 39] As shown in Table 1, the BET surface area value of the samples is 13.47 m^2/g ($Ag/AgVO_3$), 3.81 m^2/g (BiOCl) and 13.84 m^2/g (AB5.0 composite), respectively. The total pore volume of the $Ag/AgVO_3$, BiOCl and AB5.0 composite is 0.029 cm^3/g, 0.014 cm^3/g and 0.035 cm^3/g, respectively. In a word, AB5.0 composite possesses larger specific surface area and pore volume, which could improve the adsorption of dye molecules and enhance the photocatalytic activity.[36, 37]

3.6 Photoluminescence spectra analysis

Photoluminescence (PL) spectra have been widely used to disclose the migration, transfer, and separation efficiency of the photogenerated charge carriers in the semiconductor materials.[35] Lower PL intensity indicates the lower recombination of the charge carriers, implying that the more electrons and holes can take part in the oxidation and reduction reactions, resulting in the higher photocatalytic activity.[40, 41] In Fig. 6, all samples were studied by the PL spectra analysis with an excitation wavelength of 384 nm. The main emission peak center at visible light area about 771 nm can be ascribed to the band gap recombination of electron-hole pairs. The relative intensity of $Ag/AgVO_3$/BiOCl composite is lower than that of the pure BiOCl,

implying that $Ag/AgVO_3$ formed on the surface of BiOCl could efficiently inhibit the recombination of electrons and holes, which is attributed to the efficient charge transfer between BiOCl and $Ag/AgVO_3$.[27] The emission intensity of PL spectra for $Ag/AgVO_3$/BiOCl composite is in the order of AB10.0 > AB2.5 > AB5.0. The result proves that $Ag/AgVO_3$/BiOCl composite with suitable proportion is very effective for the suppression of electron-hole pair recombination, which is a necessary factor for improving the degradation of MB.[33]

3.7 Photocatalytic degradation performance

To determine the photocatalytic activity of as-prepared samples, the degradation of MB was investigated under visible light irradiation. Before light irradiation, we did a dark experiment with the composite to investigate the adsorption-desorption equilibrium (Fig. S2). After 1 h, the adsorption-desorption equilibrium has been achieved. Then, the following degradation test was carried out. Fig. 7a presented the variation of the MB concentration (C_t/C_0) according to the irradiation time over different samples. A blank experiment without any photocatalyst was also conducted for comparison. The MB degradation efficiency of AB2.5, AB5.0 and AB10.0 composite is 73.51%, 93.16% and 87.33%, respectively, which are all better than that of the pure BiOCl (29.24%) and $Ag/AgVO_3$ (37.52%).

The enhanced photocatalytic activity may be ascribed to these four reasons. (1) The presence of $Ag/AgVO_3$ greatly extended the scale of light absorption and remarkably enhanced the intensity of light absorption than pure BiOCl. (2) For BiOCl, MB dye molecules can easily adsorb on the surface of BiOCl and further be degraded

under visible light irradiation due to the dye sensitization.[14] The flowerlike hierarchical microstructure can not only enhance the surface area, but also facilitate the transfer of the dye molecules during photocatalytic process.[15, 42] With the combination of BiOCl, the separation of photogenerated electron-hole pairs and the transportation of electrons were efficiently facilitated than pure $Ag/AgVO_3$.[43] (3) For Ag nanoparticles, as it has the excellent conductivity and strong electron trapping ability (by *Zhao et al.* with fluorescence emission spectra analysis[28]), the separation of electrons and holes could be improved, as well as the interfacial charge transfer.[29] And the modified Ag nanoparticles can induce localized surface plasmon resonance (SPR) from the collective oscillation of the surface electrons and remarkably enhance the absorption of the samples in the visible light, resulting in the better photocatalytic performance (by *Zhao et al.* with UV-vis adsorption spectra analysis).[28] (4) Moreover, large specific surface area could prevent the agglomeration of BiOCl microspheres, facilitate the transfer of the dye molecules during photocatalytic process and improve the surface reaction rates.[15, 42]

To quantitatively understand the reaction kinetics of the MB solution degradation, the pseudo-first-order kinetics model was used to fit the curves:

$$-\ln(C_t/C_0) = kt \qquad (2)$$

Where k (min^{-1}) and t (min) are the apparent first-order rate constant and irradiation time, C_0 (mg/L) and C_t (mg/L) are the initial concentration of MB and the remaining concentration of MB at each time, respectively. The model fitting plots and corresponding k values are shown in Fig. 7b. It was indicated that the value of k was

in the order of AB5.0 > AB10.0 > AB2.5 > $Ag/AgVO_3$ > BiOCl with the value of 0.04437, 0.03523, 0.02153, 0.00675 and 0.00493 min^{-1}, respectively. The sequence demonstrated that the photocatalytic activity of $Ag/AgVO_3$/BiOCl composite was closely related to the amount of BiOCl. With the increase of BiOCl amount (10%), it would lead to a decrease of the photocatalytic efficiency, for the reason that the excessive BiOCl would widen the bandgap of photocatalytic composite and weaken the availability under visible light irradiation.[15] And the *k* of AB5.0 composite was 9 times than that of pure BiOCl, presenting the outstanding photocatalytic prosperity of AB5.0 composite. The temporal evolution of the spectral changes of the MB over the optimum AB5.0 photocatalyst was also detected and depicted in the Fig. 7c. MB dye manifested a maximum absorption band at 664 nm. The concentration of the MB at 664 nm was continuously decreased with the time and approached to zero after 60 min, which implied the degradation of auxochrome group of MB dye.[44] And Fig. 7d discussed the effect of different dosage of photocatalyst for the degradation of MB. The degradation rate of MB was associated with the amount of active sites in the $Ag/AgVO_3$/BiOCl photocatalytic oxidation systems. The degradation rate was limited at low dosage, for active sites were not enough. With the dosage of photocatalyst increased, the photocatalytic activity improved. However, this beneficial effect would drop off when the dosage was excess, for the penetration of visible light irradiation was weakened. The result demonstrated that the photocatalytic activity was determined by the amount of active sites and the penetration of visible light irradiation.[45] The optimum dosage is 0.5 g/L.

3.8 Possible photocatalytic mechanism

The photocatalytic activity depended on the generation, transfer and separation of photogenerated electron-hole pairs. Band positions of $Ag/AgVO_3$ and BiOCl were calculated by the following empirical formulas[33]:

$$E_{VB} = X - E^e + 0.5Eg \quad (3)$$

$$E_{CB} = E_{VB} - Eg \quad (4)$$

Where E_{VB} is the valence band edge potential, E_{CB} is the conduction band edge potential, X is the electronegativity of the semiconductor, which is the geometric mean of the electronegativity of the constituent atoms, E^e is the energy of free electrons on the hydrogen scale (about 4.5 eV), and Eg is the bandgap energy of the semiconductor. The X value of $AgVO_3$ and BiOCl is 5.86 eV and 6.46 eV, respectively. As shown in Table. 1, according to the calculation, the VB and CB edge potentials of $Ag/AgVO_3$ are 2.41 eV and 0.31 eV, respectively. And the VB and CB edge potentials of BiOCl are 3.52 eV and 0.40 eV, respectively. The result is consistent with former reports.[16, 27] To further investigate the photocatalytic mechanism, EDTA, isopropanol (IPA) and methyl alcohol (MeOH) were respectively introduced as the scavenger to quench active holes (h^+), hydroxyl radicals (•OH) and superoxide radicals ($•O_2^-$), respectively. As shown in Fig. 8a-b, in the presence of EDTA, the degradation of MB was inhibited significantly compared with no scavenger, indicating that the crucial active specie was active holes (h^+). Furthermore, the photocatalytic degradation rate also decreased with the addition of IPA and MeOH, suggesting that both •OH and $•O_2^-$ species were also participated in photocatalysis reactions.

On the basis of the above-described experimental results, the mechanism of photocatalytic degradation of MB dye over the $Ag/AgVO_3/BiOCl$ composite under visible light irradiation is proposed, as illustrated in Fig. 9. When $Ag/AgVO_3/BiOCl$ composite was subjected to visible light irradiation, the electrons (e^-) can be excited from the valence band (VB) to the conduction band (CB) of $Ag/AgVO_3$, leaving behind a hole in the valence band simultaneously. However, BiOCl can hardly be excited by visible light due to the wide band gap energy.[14] Because the CB of $Ag/AgVO_3$ (0.31 eV) was more negative than that of BiOCl (0.40 eV), the excited electrons on the CB of $Ag/AgVO_3$ would flow into the CB of BiOCl.[26] The MB molecules adsorbed on the surface of BiOCl were excited by visible light irradiation to generate electrons and then the electrons were injected from the excited MB molecules to the CB of BiOCl.[14] Thus, the electron-hole pairs were separated effectively. Then, electrons in the $Ag/AgVO_3/BiOCl$ composite can be trapped by O_2 to form $\bullet O_2^-$ reactive species, followed by the generation of •OH.[24] Lastly, these reactive species, including $\bullet O_2^-$, •OH and h^+, could directly oxidize MB dye molecules.

$$Ag/AgVO_3 + visible\ light \rightarrow Ag/AgVO_3\ (e^- + h^+) \quad (5)$$

$$AgVO_3\ (e^-) + Ag \rightarrow AgVO_3 + Ag\ (e^-) \quad (6)$$

$$Ag/AgVO_3\ (e^-) + BiOCl \rightarrow Ag/AgVO_3 + BiOCl\ (e^-) \quad (7)$$

$$MB + visible\ light \rightarrow MB^+ + e^- \quad (8)$$

$$e^- + absorbed\ O_2 \rightarrow \bullet O_2^- \quad (9)$$

$$(h^+, \bullet O_2^-, \bullet OH) + MB\ dye \rightarrow degradation\ products \quad (10)$$

3.9 Recyclability and stability

The stability of catalysts is an important issue for their practical applications. Therefore, the degradation of MB by AB5.0 composite photocatalyst was reused for five runs under same condition. As shown in Fig. 10a, the photocatalytic activity of AB5.0 composite photocatalyst remained almost unchanged after five cycles, confirming the good recyclability. The XRD pattern of the used AB5.0 sample was compared with that of the fresh AB5.0 sample (Fig. 10b). As we have seen, the intensity of Ag in the used AB5.0 sample is higher than that of in the fresh AB5.0 sample, indicating the increase of Ag nanoparticles. The result is consistent with the report of *Zhao et al.* Ag nanoparticles may be generated under light irradiation for the photosensitivity of silver ion.[38, 46]

4. Conclusions

In summary, a novel Ag/$AgVO_3$/BiOCl composite photocatalyst was initiated via a facile ultrasound assisted hydrothermal method. BiOCl microspheres were uniformly dispersed and integrated with Ag/$AgVO_3$ microrods. The photocatalytic activity for MB degradation was investigated under visible light irradiation. The Ag/$AgVO_3$/BiOCl composite photocatalyst exhibited a much higher photocatalytic activity than pure BiOCl and Ag/$AgVO_3$. Especially, the degradation efficiency of AB5.0 composite is 93.16% within 60 min. The enhanced photocatalytic activity could be attributed to the effective visible light absorption, charge transportations and efficient separations. The Ag/$AgVO_3$ microrods greatly extended the scale of light absorption and remarkably enhanced the intensity of light absorption. The BiOCl

microspheres acted as a transporter to separate photogenerated electron-hole pairs. And the modified Ag nanoparticles can induce localized surface plasmon resonance (SPR) from the collective oscillation of the surface electrons and remarkably enhance the absorption of the samples in the visible light. Active holes (h^+) as dominant active species generated during the photocatalytic process were ordered to interact with the pollutants. In addition, Ag/$AgVO_3$/BiOCl composite photocatalyst exhibited excellent stability. The synergetic effect between noble metal oxide and semiconductor enlightened more possibility about the potential application in the field of wastewater treatment.

Acknowledgements

The authors gratefully acknowledge the financial support provided by Collaborative Innovation Center of Resource-Conserving & Environment-friendly Society and Ecological Civilization, the National Natural Science Foundation of China (No. 71431006, 21276069).

References

1. H. Wang, X. Yuan, Y. Wu, H. Huang, X. Peng, G. Zeng, H. Zhong, J. Liang and M. Ren, *Adv. Colloid Interface Sci.*, 2013, **195-196**, 19-40.
2. H. Wang, X. Yuan, G. Zeng, Y. Wu, Y. Liu, Q. Jiang and S. Gu, *Adv. Colloid Interface Sci.*, 2015, **221**, 41-59.
3. N. Wetchakun, S. Chainet, S. Phanichphant and K. Wetchakun, *Ceram. Int.*, 2015, **41**, 5999-6004.
4. C. Dong, X. Xiao, G. Chen, H. Guan and Y. Wang, *Mater. Chem. Phys.*, 2015, **155**, 1-8.
5. J. R. Reddy, S. Kurra, R. Guje, S. Palla, N. K. Veldurthi, G. Ravi and M. Vithal, *Ceram. Int.*, 2015, **41**, 2869-2875.
6. X. Wen and L. Tang, *J. Mol. Catal. A: Chem.*, 2015, **399**, 86-96.
7. A. Singh, D. P. Dutta, A. Ballal, A. K. Tyagi and M. H. Fulekar, *Mater. Res. Bull.*, 2014, **51**, 447-454.
8. H. Wang, X. Yuan, Y. Wu, G. Zeng, X. Chen, L. Leng, Z. Wu, L. Jiang and H. Li, *J. Hazard. Mater.*, 2015, **286**, 187-194.
9. X. Yuan, H. Wang, Y. Wu, X. Chen, G. Zeng, L. Leng and C. Zhang, *Catal. Commun.*, 2015, **61**, 62-66.
10. H. Wang, X. Yuan, Y. Wu, G. Zeng, X. Chen, L. Leng and H. Li, *Appl. Catal. B Environ.*, 2015, **174-175**, 445-454.
11. H. Wang, X. Yuan, Y. Wu, X. Chen, L. Leng and G. Zeng, *RSC Adv.*, 2015, **5**, 32531-32535.

12. Z. Zarghami, M. Ramezani and M. Maddahfar, *Mater. Lett.*, 2015, **152**, 21-24.

13. M. Zhang, Y. Liu, L. Li, H. Gao and X. Zhang, *Catal. Commun.*, 2015, **58**, 122-126.

14. K. Li, Y. Tang, Y. Xu, Y. Wang, Y. Huo, H. Li and J. Jia, *Appl. Catal. B Environ.*, 2013, **140-141**, 179-188.

15. K. Wang, C. Shao, X. Li, X. Zhang, N. Lu, F. Miao and Y. Liu, *Catal. Commun.*, 2015, **67**, 6-10.

16. F. Duo, Y. Wang, X. Mao, X. Zhang, Y. Wang and C. Fan, *Appl. Surf. Sci.*, 2015, **340**, 35-42.

17. L. Li, M. Zhang, Y. Liu and X. Zhang, *J. Colloid Interface Sci.*, 2014, **435**, 26-33.

18. Y. Mi, L. Wen, Z. Wang, D. Cao, Y. Fang and Y. Lei, *Appl. Catal. B Environ.*, 2015, DOI: 10.1016/j.apcatb.2015.04.013.

19. X. Gao, X. Zhang, Y. Wang, S. Peng, B. Yue and C. Fan, *Chem. Eng. J.*, 2015, **263**, 419-426.

20. J. Cao, C. Zhou, H. Lin, B. Xu and S. Chen, *Appl. Surf. Sci.*, 2013, **284**, 263-269.

21. Y. Zuo, C. Wang, Y. Sun and J. Cheng, *Mater. Lett.*, 2015, **139**, 149-152.

22. Y. Liu, X. Yuan, H. Wang, X. Chen, S. Gu, Q. Jiang, Z. Wu, L. Jiang and G. Zeng, *RSC Adv.*, 2015, **5**, 33696-33704.

23. V. Sivakumar, R. Suresh, K. Giribabu and V. Narayanan, *Solid State Sci.*, 2015, **39**, 34-39.

24. P. Ju, H. Fan, B. Zhang, K. Shang, T. Liu, S. Ai and D. Zhang, *Sep. Purif. Technol.*, 2013, **109**, 107-110.

25. J. Ren, W. Wang, M. Shang, S. Sun, L. Zhang and J. Chang, *J. Hazard. Mater.*, 2010, **183**, 950-953.

26. W. Zhao, Y. Guo, Y. Faiz, W.-T. Yuan, C. Sun, S.-M. Wang, Y.-H. Deng, Y. Zhuang, Y. Li, X.-M. Wang, H. He and S.-G. Yang, *Appl. Catal. B Environ.*, 2015, **163**, 288-297.

27. W. Zhao, Y. Guo, S. Wang, H. He, C. Sun and S. Yang, *Appl. Catal. B Environ.*, 2015, **165**, 335-343.

28. W. Zhao, J. Li, Z. b. Wei, S. Wang, H. He, C. Sun and S. Yang, *Appl. Catal. B Environ.*, 2015, **179**, 9-20.

29. X. Hu, C. Hu and J. Qu, *Mater. Res. Bull.*, 2008, **43**, 2986-2997.

30. X. Zhang, T. Guo, X. Wang, Y. Wang, C. Fan and H. Zhang, *Appl. Catal. B Environ.*, 2014, **150-151**, 486-495.

31. H.-Y. Hao, Y.-Y. Xu, P. Liu and G.-Y. Zhang, *Chin. Chem. Lett.*, 2015, **26**, 133-136.

32. J. Cao, B. Xu, H. Lin, B. Luo and S. Chen, *Catal. Commun.*, 2012, **26**, 204-208.

33. F. Duo, Y. Wang, C. Fan, X. Mao, X. Zhang, Y. Wang and J. Liu, *Mater. Charact.*, 2015, **99**, 8-16.

34. H. Xu, H. Li, G. Sun, J. Xia, C. Wu, Z. Ye and Q. Zhang, *Chem. Eng. J.*, 2010, **160**, 33-41.

35. X. Lin, X. Guo, W. Shi, F. Guo, H. Zhai, Y. Yan and Q. Wang, *Catal. Commun.*, 2015, **66**, 67-72.

36. C. Huang, J. Hu, S. Cong, Z. Zhao and X. Qiu, *Appl. Catal. B Environ.*, 2015, **174-175**, 105-112.

37. F. Dong, Y. Sun, M. Fu, Z. Wu and S. C. Lee, *J. Hazard. Mater.*, 2012, **219-220**, 26-34.

38. C. Belver, C. Adán, S. García-Rodríguez and M. Fernández-García, *Chem. Eng. J.*, 2013, **224**, 24-31.

39. L.-P. Zhu, G.-H. Liao, N.-C. Bing, L.-L. Wang, Y. Yang and H.-Y. Xie, *CrystEngComm*, 2010, **12**, 3791.

40. F. Xie, X. Mao, C. Fan and Y. Wang, *Mater. Sci. Semicond. Process.*, 2014, **27**, 380-389.

41. G.-T. Pan, C.-M. Huang, P.-Y. Peng and T. C. K. Yang, *Catal. Today.*, 2011, **164**, 377-383.

42. Y. Mi, L. Wen, Z. Wang, D. Cao, Y. Fang and Y. Lei, *Appl. Catal. B Environ.*, 2015, **176-177**, 331-337.

43. K. Zhang, C. Liu, F. Huang, C. Zheng and W. Wang, *Appl. Catal. B Environ.*, 2006, **68**, 125-129.

44. X. Yu, L. Huang, Y. Wei, J. Zhang, Z. Zhao, W. Dai and B. Yao, *Mater. Res. Bull.*, 2015, **64**, 410-417.

45. X. Gao, X. Zhang, Y. Wang, S. Peng, B. Yue and C. Fan, *Chem. Eng. J.*, 2015, **273**, 156-165.

46. L. Xu, Y. Wei, W. Guo, Y. Guo and Y. Guo, *Appl. Surf. Sci.*, 2015, **332**, 682-693.

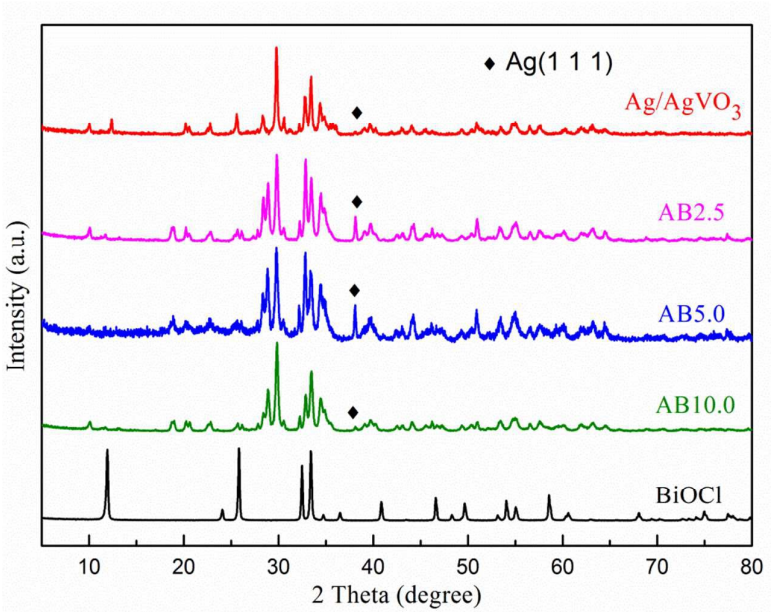

Fig. 1 XRD pattern of the $Ag/AgVO_3$, AB2.5, AB5.0, AB10.0 and BiOCl samples.

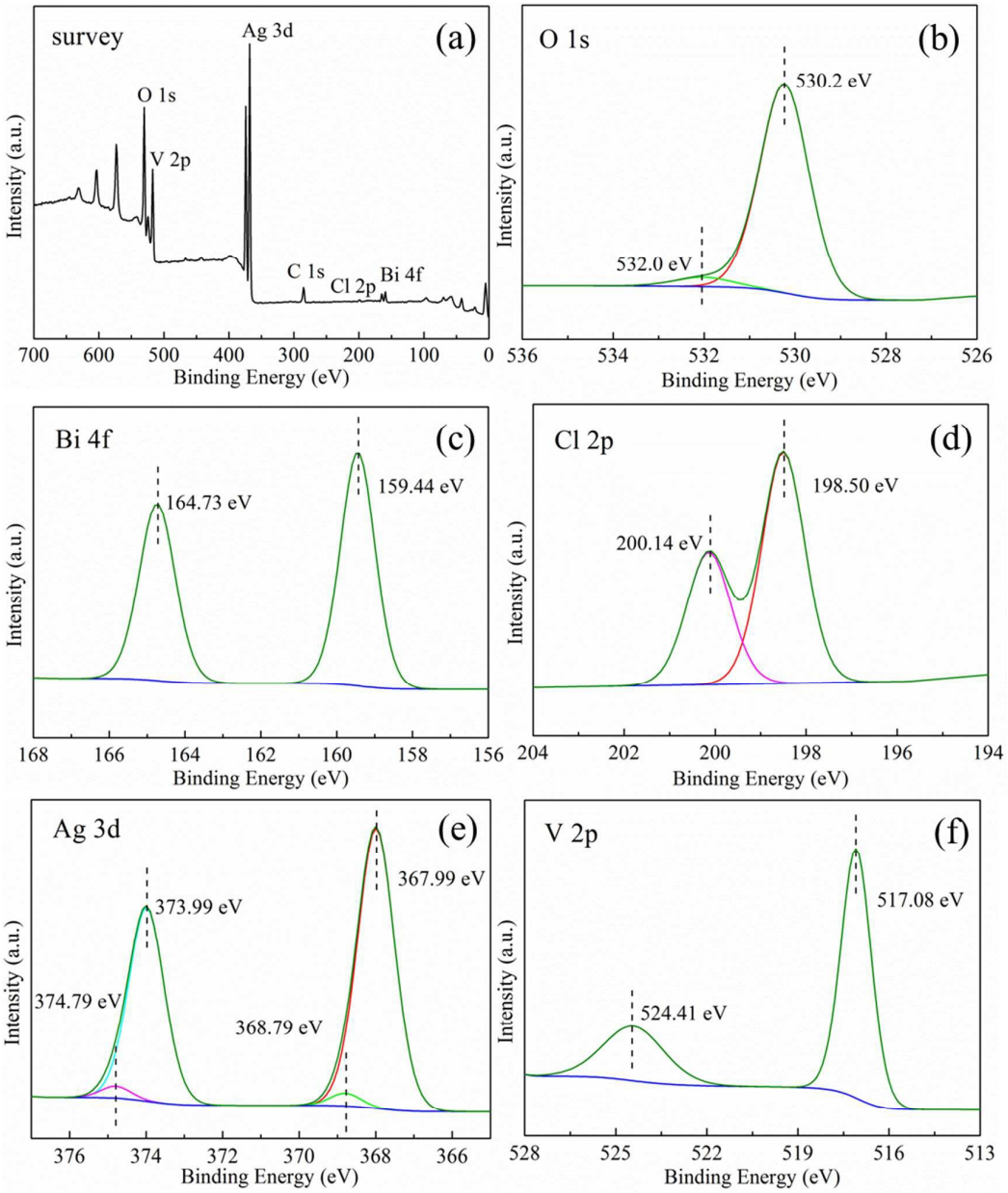

Fig. 2 XPS spectra of the as-synthesized AB5.0 sample: (a) survey scan, (b) O 1s, (c) Bi 4f, (d) Cl 2p, (e) Ag 3d, and (f) V 2p.

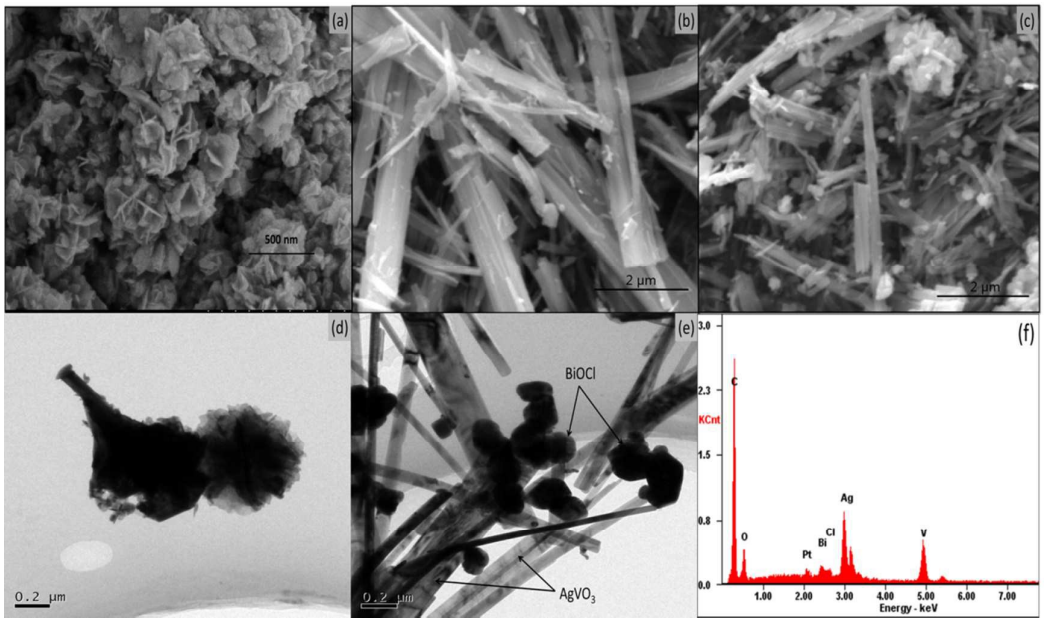

Fig. 3 SEM images of (a) BiOCl, (b) $Ag/AgVO_3$, and (c) AB5.0 samples; TEM images of (d) BiOCl and (e) AB5.0 samples; EDS spectrum of (f) AB5.0 sample.

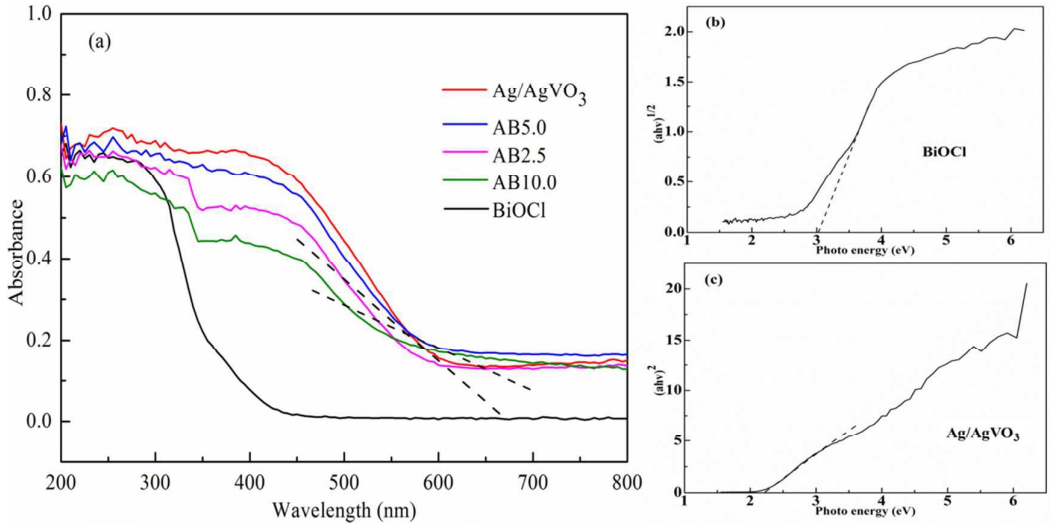

Fig. 4 (a) UV-vis diffuse reflectance spectra of different samples; the band gap energy of (b) BiOCl and (c) $Ag/AgVO_3$samples

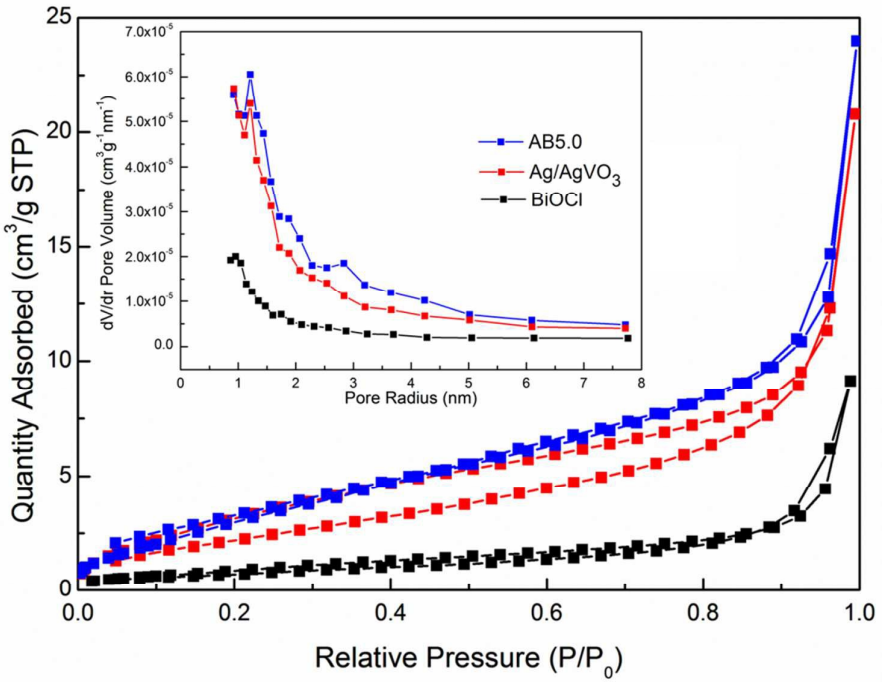

Fig. 5 N_2 adsorption-desorption isotherms of the $Ag/AgVO_3$, BiOCl and AB5.0 samples. Inset: the corresponding pore-size distribution.

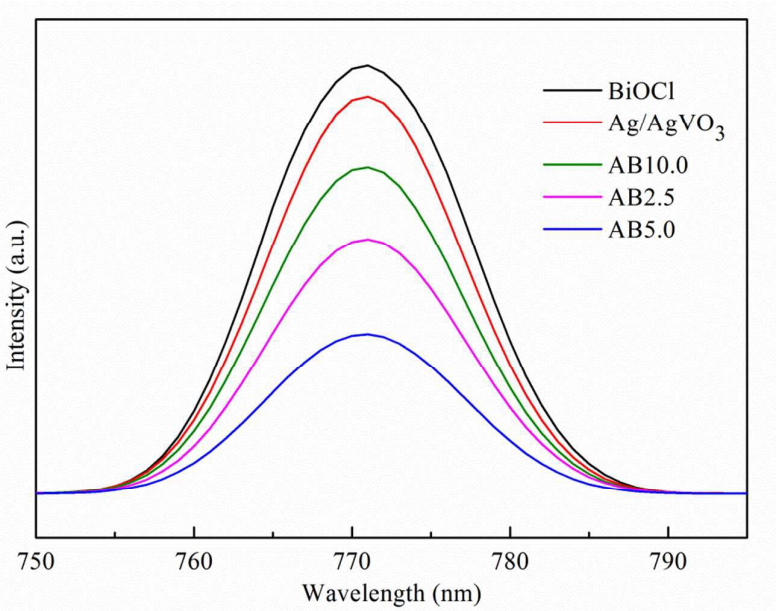

Fig. 6 PL spectra of as-prepare samples with the excitation wavelength of 384 nm

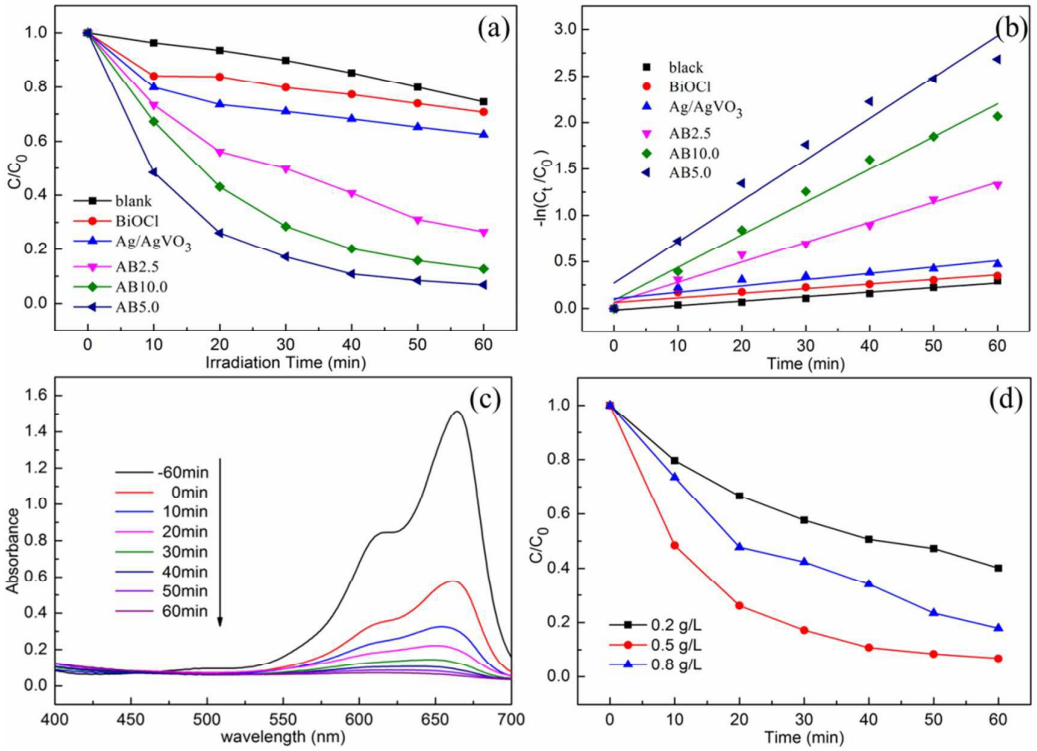

Fig. 7 (a) Photocatalytic degradation of MB over different samples under visible light irradiation; (b) Pseudo first-order kinetics fitting plots; (c) UV-vis absorption spectra changes of MB over the AB5.0 composite in every 10 min under visible light irradiation; (d) Photocatalytic degradation of MB over different dosage of AB5.0.

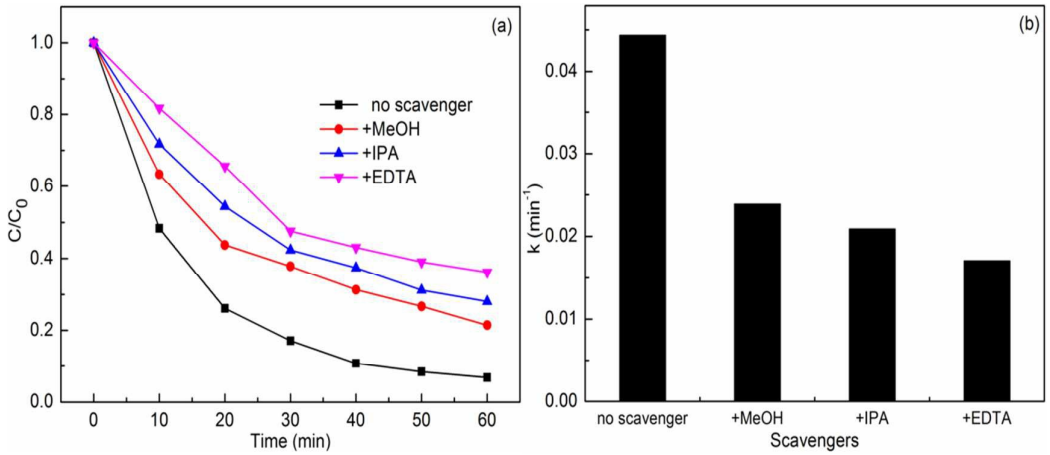

Fig. 8 (a) Effects of different reactive species scavengers on the photocatalytic degradation of MB by AB5.0 under visible light irradiation; (b) Histogram of k value.

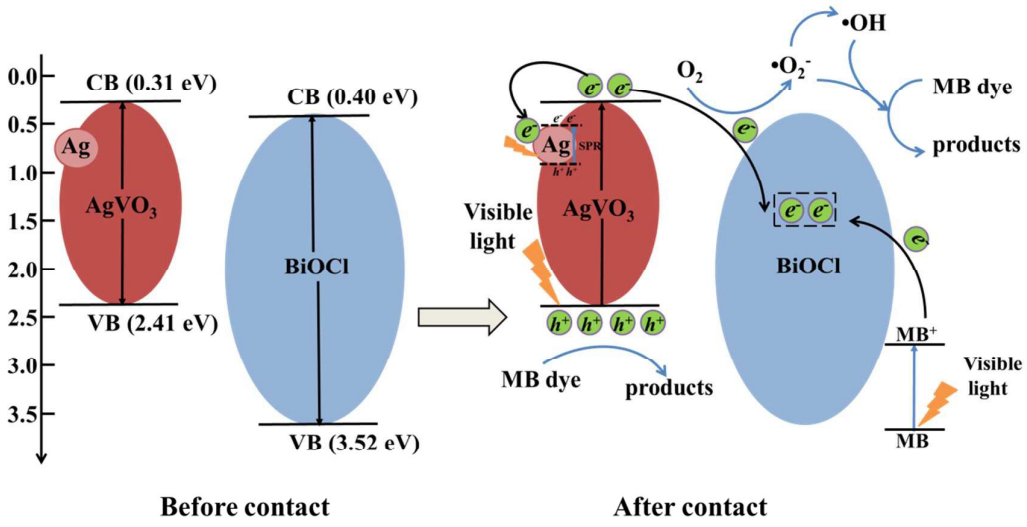

Fig. 9 Schematic illustration of band structures and possible photocatalytic reactions of $Ag/AgVO_3/BiOCl$ photocatalyst

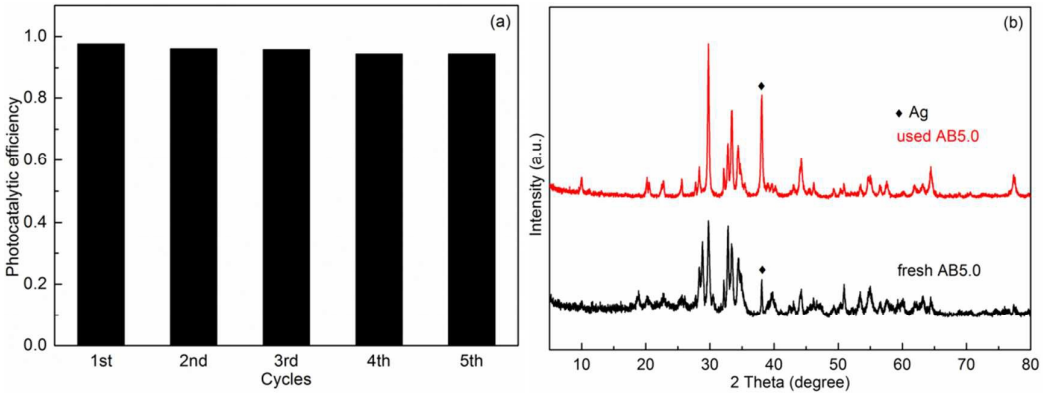

Fig. 10 (a) Cycles for five times in the presence of AB5.0 under visible light irradiation; (b) XRD patterns of used AB5.0 sample and fresh AB5.0 sample.

Table 1

BET surface area and total pore volume of $Ag/AgVO_3$, BiOCl and AB5.0 samples; The calculated values of energy bandgap (Eg), valence band edge potential (E_{VB}) and conduction band edge potential (E_{CB}) of $Ag/AgVO_3$ and BiOCl samples.

Samples	BET characterization		Optical property (eV)		
	Surface area (m^2/g)	Total pore volume (cm^3/g)	Eg	E_{VB}	E_{CB}
$Ag/AgVO_3$	13.47	0.029	2.10	2.41	0.31
BiOCl	3.81	0.014	3.12	3.52	0.40
AB5.0	13.84	0.035			